Meteorological Results from Multi-Spectral Photometry in Airglow Bands by the OGO-4 Satellite

GUENTER WARNECKE,[1] EDITH I. REED AND WALTER B. FOWLER

Goddard Space Flight Center, Greenbelt, Md.

EARL R. KREINS, Major, USAF[2]

USAF Environmental Technical Applications Center, Washington, D. C.

LEWIS J. ALLISON

Goddard Space Flight Center, Greenbelt, Md.

AND JAQUES E. BLAMONT

Centre National de la Recherche Scientifique, Paris, France

(Manuscript received 30 August 1968, in revised form 20 June 1969)

ABSTRACT

The presence or absence of clouds, their characteristics, and variations of surface albedo have been correlated with observations made at several different wavelengths in the visible spectrum. These were made at high and low nighttime light levels by an airglow photometer aboard the OGO-4 satellite during August 1967 through January 1968. The wavelength regions studied were approximately 50 Å bands centered at 3914, 5577, 5893, 6225 and 6300 Å, in the energy range of 10^{-7} to 10^{-3} erg cm^{-2} sec^{-1} Å^{-1} ster^{-1} with a field of view of ~10 degrees. It was found that at the longer wavelengths (6225 and 6300 Å) the observations were strongly influenced by the variations of surface albedo. At the shorter wavelengths, the surface albedo variations were partly masked by the light returned through Rayleigh and Mie scattering. Preliminary analysis is made of surface and clouds by study of reflective radiance under moonlight and other nocturnal illuminations. Possibilities of further analysis are examined including methods of deducing cloud height information.

1. Introduction

From August 1967 through January 1968, an airglow photometer aboard a Polar Orbiting Geophysical Observatory (OGO-4) observed the night side of the earth in a number of different wavelengths in the visible spectrum. It was flown for the purpose of studying airglow, a luminescence of the atmosphere dimly visible to the naked eye. Besides the light from the airglow, the photometer unavoidably also observed the light emitted by various other natural and artificial sources, such as aurora and city street lights, and in addition, the moonlight, starlight and zodiacal light, reflected from the cloud-covered earth. A careful study was made of these nighttime observations to determine their usefulness in detecting the presence and absence of clouds, cloud top heights, and surface albedo.

Hitherto, satellite observations of the nightside for meteorological purposes have used only IR techniques, although the Mercury and Gemini astronauts were able to discern clouds under no-moon conditions (Dunkelman, 1968). The cloud mapping by Nimbus High Resolution Infrared Radiometer (HRIR) measurements was a decisive step in the development of a meteorological observation system from space. Although IR measurements can be used to infer cloud top altitudes from the derived cloud top temperatures, measurements in the visible part of the spectrum also should, at least in theory, provide both cloud coverage and cloud top heights. Suomi and Parent (1968) suggested the evaluation of cloud pictures taken in three different spectral regions of the visible by the ATS-III Multi-Color Spin Scan Cloud Camera to derive cloud top heights at least near the terminator. The OGO-4 airglow experiment with its high sensitivity and much narrower spectral bandwidth, however, provided data which allow one to explore the possibilities of deriving cloud coverage and cloud top altitude information from

[1] On leave from Freie Universität Berlin, Germany, as a National Academy of Sciences–National Research Council Senior Postdoctoral Resident Research Associate with the the National Aeronautics and Space Administration. Present Affiliation: Institut fuer Theoretische Meteorologie, Freie Universitat Berlin, Germany.

[2] Air Weather Service member temporarily attached to Goddard Space Flight Center. Present affiliation: Headquarters, U. S. Air Force, Joint Meteorological Satellite Program Office, Washington, D. C.

TABLE 1. Optical characteristics of the airglow photometer. The conversion factor for a continuum is in ergs cm^{-2} sec^{-1} $Å^{-1}$ $ster^{-1}V^{-1}$ and for line emission is in Rayleighs per volt. The area of the field of view is in steradians.

Channel	Nominal wavelength (Å)	Conversion factor		Effective bandpass	Field of view	
		Continuum	Line		Half angle	Area
1	2630	3.7×10^{-7}		258	4°51′	0.0220
2	6300	1.19×10^{-6}	195	40	3°23′	0.0109
3	6300	5.66×10^{-7}	99	44	4°27′	0.0190
4	6225	4.12×10^{-7}		59.5	4°42′	0.0211
5	5892	4.32×10^{-7}	75.8	45	4°54′	0.0229
6	5577	2.6×10^{-7}	51.3	57	4°41′	0.0210
7	3914	3.4×10^{-7}	49.3	49	4°52′	0.0227
	dark current					

multi-spectral measurements in the visible, even under nighttime conditions, from satellite altitudes.

2. The airglow experiment

The OGO-4 photometer (Reed and Blamont, 1967) used a single photomultiplier to measure incident light in both the nadir and zenith directions at various wavelengths by selecting a different interference filter or light path in a continuous cycle. The appropriate mirrors were switched at 1-sec intervals so that a complete cycle of measurements (eight channels) occurred every 8 sec. During the time for one cycle of measurements, the satellite moved $\sim 0.5°$ latitude.

The spectral characteristics of the photometer are given in Tables 1 and 2. Channels 1 and 4 were for the purpose of looking at spectral regions in the vicinity of the listed nominal wavelengths. The remaining channels were chosen to monitor specific emission lines of the airglow and aurora. For convenience in studies of continuum sources, such as the moon and stars, conversion factors are given in ergs cm^{-2} sec^{-1} $Å^{-1}$ $ster^{-1}$ V^{-1}. For airglow and aurora studies, the conversion factors are also given in Rayleighs per volt at the nominal wavelength. One Rayleigh is an apparent emission rate of 1 megaphoton cm^{-2} (column) sec^{-1}. These factors are based on laboratory calibrations several months before launch. There is some indication of shift after launch such as to make the values in this table minimum values. The effective spectral bandpass, as well as the shape of the associated relative response curve, is given in the two tables. The field of view, stated in terms of half-angles and in steradians, gave a ground coverage of 70–160 km depending on whether the satellite was at perigee or apogee, which were 408 and 908 km, respectively.

In one of the eight channels (No. 0) the field of view was blocked to establish the level of the background current. Channel No. 1 was for the measurement of middle UV emissions. Absorption at these wavelengths by atmospheric ozone blocks the underlying characteristics of clouds and earth's surface. Channel No. 2 viewed the sky above the spacecraft and was the only channel viewing in the zenith direction, all others viewed in the nadir direction. The data from the remaining five channels are in or near the visible wavelength region and measured, in addition to atmospheric emissions, radiance from the earth's surface and cloud structures. These five channels were centered at wavelengths of particular significance for airglow studies. The emission features of interest were as follows, ranging from the blue end of the spectrum to the red:

3914 Å The second positive system of N_2^+, characteristic of aurora. Outside of the auroral regions, weak Herzberg and Chamberlain bands are within the bandwidth of this filter.

5577 Å The forbidden green line of atomic oxygen, enhanced in aurora.

5893 Å The yellow sodium doublet at 5890Å and 5896Å.

6225 Å For background determination. OH emissions in this interval are sometimes quite strong.

6300 Å One of the forbidden red lines of atomic oxygen, enhanced in aurora.

These emissions all originate at altitudes ranging from 60 to 1000 km.

TABLE 2. Spectral characteristics of each channel.

Channel	Wavelength (Å) at stated relative responsivity						
	0.01	0.1	0.5	1.0	0.5	0.1	0.01
1	2250	2436	2554	2652	2778	2920	3118
2	6240.5	6267	6284.5	6303	6319.5	6336.2	6364
3	6238.5	6262.3	6279.0	6298.5	6319.5	6334.5	6360.5
4	6139.5	6179.7	6201.7	6229.5	6257.0	6279.7	6320.7
5	5818.8	5846.0	5864.0	5885.0	5905.5	5921.7	5951.7
6	5487	5526.8	5549.0	5574.0	5600.2	5625.5	5670
7	3847.5	3881.0	3900.2	3924.5	3946.2	3965.0	3997

3. The meteorological significance of the experiment

a. Theoretical considerations

When looking toward the earth in visible and near visible wavelengths, the instrument detects both primary and secondary radiation. Primary radiation is defined as the emissions originating in the earth's atmosphere such as airglow (A), and aurora (P), as well as surface lights, most noticeably, cities. The locations of cities are well known and can be separated from the data as required. Secondary radiation, or that which is reflected or scattered upward from the earth's surface and lower atmosphere, is dependent on the downward-directed radiance integrated over the hemisphere of the sky. The surface can be illuminated not only by airglow and auroral emissions but also by the moon (M), the stars (S), and zodiacal light (Z). The airglow is an extended source which varies as a function of zenith angle; stars, zodiacal light and aurora are quasi-extended sources; the moon may be treated as a point source. When the effects of scattering and absorption are also taken into account, the statement of the relationship between these sources and the total upward radiance viewed by the photometer becomes very complex. However, it is useful to look at the problem in a simplified manner and to define an apparent reflectivity r as the radiant reflectance of a lambert surface which gives a radiance identical to that measured. The detected radiance N can then be represented symbolically by

$$N=A+P+r(\bar{A}+\bar{M}+\bar{S}+\bar{Z}+\bar{P}), \tag{1}$$

where the bar indicates upward radiance equal to the integrated radiance falling on the lambert surface. It is to be noted that each of the above terms is a function of wavelength.

Representative values for each of these components are listed in Table 3, where the energy in the 50 Å interval centered at the nominal wavelength is given. For the airglow emissions, the average values given by Roach (1964) were used. The integrated starlight is assumed to be equal to 100 tenth-magnitude stars (visual scale) of spectral type G2 per square degree; the zodiacal light is assumed to be equivalent to 200 such stars per square degree. It is to be noted that the contributions by airglow, zodiacal light and starlight are of the same order of magnitude, and that moonlight, when present, is generally dominant.

In the case of no moonlight ($M=0$) and outside the auroral zone ($P=0$), (1) reduces to

$$N=A+r(\bar{A}+\bar{S}+\bar{Z}). \tag{2}$$

The expressions for the detected spectral radiance can be further simplified by noting that the integrated starlight and the integrated zodiacal light are nearly constant. The detected radiance is then a function of only two variables, thus

$$N=f(A,r). \tag{3}$$

The variations of the airglow and apparent reflectivity are such that the detected radiance appears to have a slowly varying component due to airglow and a rapidly varying component due to changes of apparent reflectivity. Examples of the extent to which these two components can be distinguished and useful information determined concerning the nature of the surfaces will be discussed in later sections.

In the case of moonlight, outside the auroral zone, (1) may be modified to

$$N=A+r_e(\bar{A}+\bar{S}+\bar{Z})+r_m\bar{M}. \tag{4}$$

Here, r_e represents an apparent reflectivity for a surface illuminated by extended sources and r_m an apparent reflectivity for illumination by a point source. Since the earth and lower atmosphere are, in fact, not perfect lambert surfaces, the reflectivity under the two conditions is somewhat different. The moonlight received by the detector is a function of lunar phase and elevation angle. Except near the time of new moon, whenever the moon is in the sky, the moonlight component overwhelms the components due to airglow, starlight and zodiacal light. Thus, under moonlit conditions, the observed radiance again appears to consist of two components, one of which, $\bar{M}$, changes very slowly and is due to changes in lunar phase and elevation, and the other of which changes rapidly and is due to changes in reflectivity r_m. The slowly changing component is subject to computation, and hence the detected radiance can be used to measure the apparent reflectivity r_m. Eq. (4) can then be expressed as

$$N=f(r_m). \tag{5}$$

TABLE 3. Typical radiances from nocturnal sources measured in 50 Å spectral intervals (erg sec^{-1} cm^{-2} ster^{-1}).

Source	3914 Å	5577 Å	5890 Å	6225 Å	6300 Å
$A(\lambda)$, continuum	3×10^{-6}	7×10^{-5}	1.2×10^{-5}	1.2×10^{-5}	3.0×10^{-5}
$M(\lambda)$, maximum	3×10^{-3}	6.9×10^{-3}	7.5×10^{-3}	6.6×10^{-3}	6.6×10^{-3}
$S(\lambda)$, $100s_{10}$ (vis)	3.6×10^{-6}	6.2×10^{-6}	5.9×10^{-6}	5.5×10^{-6}	5.4×10^{-6}
$Z(\lambda)$, $200s_{10}$ (vis)	7.3×10^{-6}	1.2×10^{-5}	1.2×10^{-5}	1.1×10^{-5}	1.1×10^{-5}
$P(\lambda)$			highly variable		

TABLE 4. Examples of reflectance values of some natural surfaces at 5577 Å.

Surface	Spectral reflectance	Reference
Water surface	0.05	Krinov (1947)
Green grass	0.10	Kondratiev *et al.* (1962)
Sand dunes	0.30	Krinov (1947)
Clay or limestone	0.62	Krinov (1947)
Cloud	0.72	Novoseltsev (1964)
Snow	0.75	Krinov (1947)
Snow	0.82	Kondratiev *et al.* (1962)

The apparent reflectivity depends in part on the reflectance of the cloud or earth surface and in part upon the scattering occurring in the atmosphere between the observer and the surface. Typical values of the spectral reflectance of various natural surfaces are given in Table 4. The effect of scattering is, in turn, a function of the position of the source and the observer. Since short wavelengths (e.g., 4000 Å) are scattered more strongly than those in the red (e.g., 7000 Å) a comparison of observations made at the two wavelengths should provide a measure of the depth of the reflecting surface in the atmosphere, that is, a measure of the height of cloud tops.

To make a quantitative estimate of the effect of the atmosphere, Fig. 1 was constructed from the computations of Plass and Kattawar (1968). Plotted is the ratio of the radiance observed at two different wavelengths (spectral ratio) as a function of the radiance observed at the longer wavelength. The observer is assumed to be at zenith and the source at an elevation of ~20°, typical for the observational material to be presented in the next section. For the purposes of this computation, the radiances of the source at the two wavelengths were assumed equal and the ratio received by the observer was plotted for the various surface reflectivities. The surface is assumed to be lambert (free from specular reflection) and gray (with a reflectivity which is constant as a function of wavelength). In the absence of an atmosphere, the radiance received is independent of the wavelength and its spectral ratio is equal to 1.0, as indicated in the figure by the horizontal line labeled "gray lambert surface above atmosphere." The presence of the atmosphere modifies the spectral ratio and the lower curve gives the spectral ratio for a surface at the bottom of the earth's atmosphere.

Hence, observations of moonlight reflected from gray surfaces should fall in the area bounded by these two lines and by the lines indicating 0% reflectivity of the surface. If the point is near the left side of this area, it means that the surface has a low reflectivity; if it is near the lower boundary, it means that the reflecting surface is near the base of the atmosphere, i.e., on or near the earth's surface; if it is near the upper boundary, the surface could be interpreted as clouds high in the atmosphere. It is apparent for surfaces of high reflectivity such as clouds that the height of the surface would have but little effect on the observations. Hence,

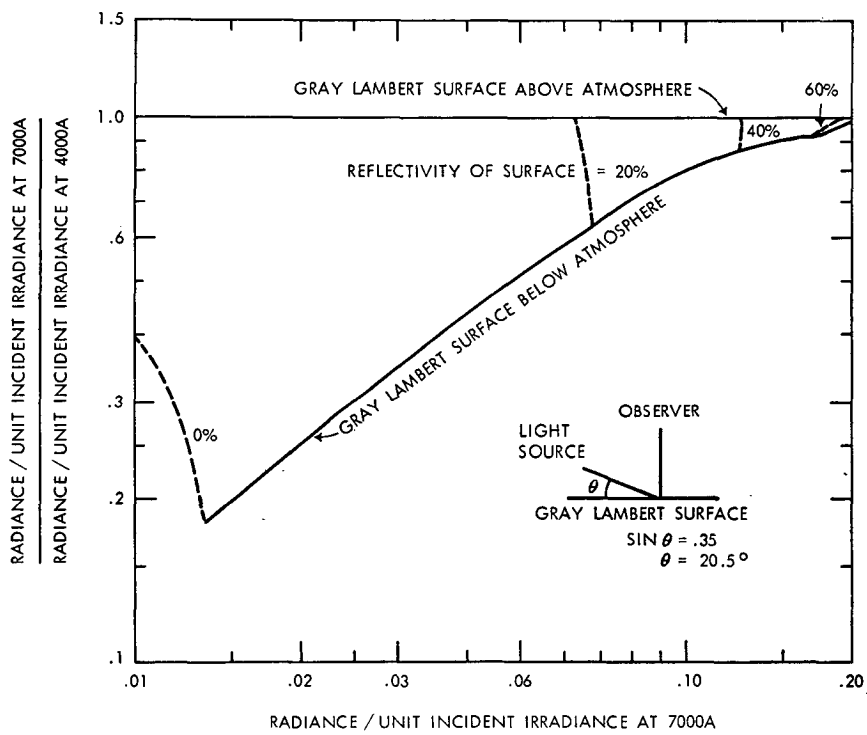

FIG. 1. The effects of the intervening atmosphere and the surface albedo on the spectral content and magnitude of radiance observable from a spacecraft.

it does not appear that one would be able to distinguish high cloud decks from low-lying surfaces which have a high albedo such as snow, sea ice, fog or very low cloud decks. But if the surface is uneven and the elevation angle of the light source is low such that a considerable portion of the surface is in shadow, then its effective reflectivity is lowered and the observed reflectivity should depend more strongly upon the height of the surface within the atmosphere.

b. Experimental results

Data from the three OGO-4 orbits have been selected for this publication covering cases of new moon and full moon primarily over Africa, where a large variety of terrestrial and cloud conditions along the meridional satellite track could be expected, and also over oceanic regions where the background is relatively homogeneous. Data obtained over arctic regions, not presented herein, indicate that the albedo is high in all wavelengths, and the variations of the observed radiance are generally less than 20%.

1) Low light levels. On orbit 507, 1 September 1967, OGO-4 on its near-midnight passage went southward along 21.9E across the Mediterranean Sea, passed the North African coast near Marsa Susa, Libya, and flew over large sections of the cloud-free Sahara Desert, and finally passed over tropical cloud systems in central Africa. Fig. 2 is an ESSA-5 television view of this area ~12 hr later. It is a reasonable assumption that the cloud distribution in this photograph is fairly representative for the time of the OGO-4 overpass. The airglow measurements for three channels are reproduced in Fig. 3. Although the moon is above the horizon, its phase and elevation are such that the illumination of the earth by the moon is comparable to that by starlight and zodiacal light.

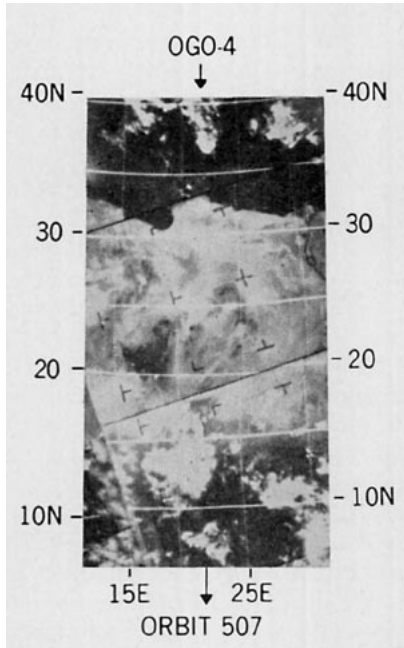

FIG. 2. Path of OGO-4 orbit 507 (indicated by arrows) superimposed on photographs from the ESSA-5 satellite, 1 September 1967, 1300 GMT, orbit 1699. Latitude and longitude are indicated at the edges of the picture. These photographs were made ~12 hr after the OGO-4 data presented in Fig. 3.

The channel centered at 3914 Å does not show any significant response to surface features like the Mediterranean coast with its remarkable change in albedo between the dark ocean and the bright desert which is very prominent in the satellite television picture. South of 16N, however, a pronounced increase in the 3914 Å radiance coincides with an extended tropical cloud system of variable density and cloud top altitudes. Over these clouds the radiance increased by an average factor of 2.0 from the clear zone. At longer wavelengths, 6225 and 5577 Å, the coastline is indicated by increases

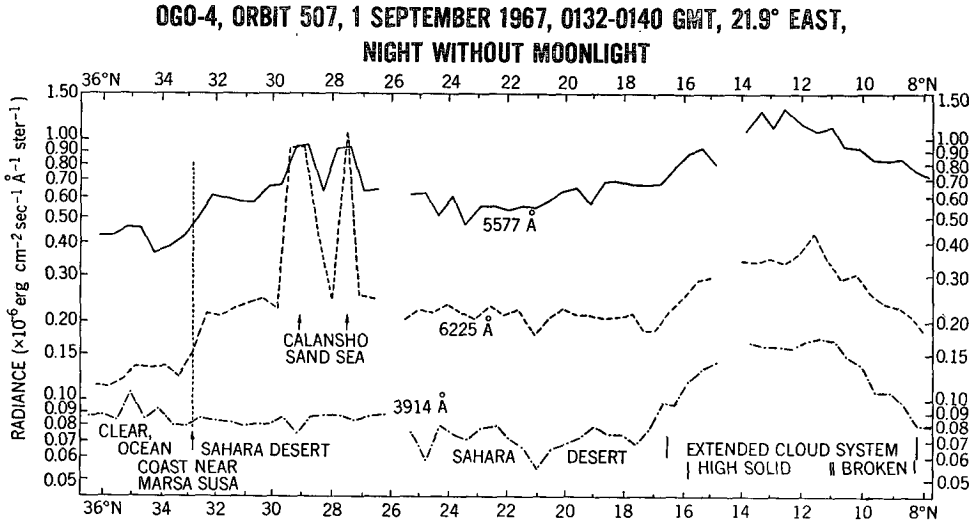

FIG. 3. Observed radiance as a function of geographic latitude.

in radiance by 1.8 and 1.5, respectively, and both the channels show continuously high values over the desert areas. A further increase by factors of 2.6 and 2.9, respectively, was observed over the tropical cloud systems previously mentioned.

This example clearly shows that without illumination by moonlight the combined intensities of reflected airglow, reflected starlight and reflected zodiacal light are sufficient for a unique differentiation between clear and cloudy regions; they do significantly show terrestrial features like brightness differences between sea and desert land. The different response of the three channels to surface features (coast line) and clouds obviously makes it possible, even under the most unfavorable condition of the absence of moonlight, to discriminate cloudy and clear areas.

An originally mysterious singularity in the airglow measurements shown in Fig. 3 occurred between 27 and 30N in the area of the Calansho Sand Sea, where two very strong peaks in the radiance recorded in the 6225 Å channel were observed. The fact of no noticeable concurrent variation in the 3914 Å channel suggests a surface phenomenon. It appears that the photometer sensed the incandescent outdoor lights and burning of excess natural gas in the oil fields newly exploited in this area.

2) Moonlight. On 20 August 1967, OGO-4 on orbit 331 passed along 26E southward over Africa under near full moon. Moon elevations increased from 11° at 40N to 26° at 5S. The ESSA-5 photograph taken 12 hr later and reproduced in Fig. 4 again shows clear skies over large parts of the Mediterranean Sea and the North African deserts. Between 20N and the equator, clouds of various horizontal and presumably different vertical extent were beneath the subsatellite track.

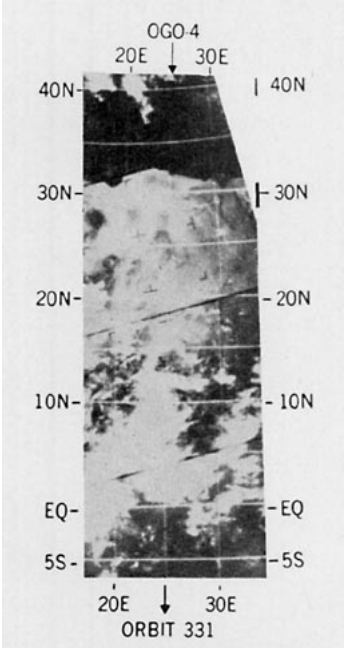

FIG. 4. Path of OGO-4 orbit 331 superimposed on photographs from the ESSA satellite, 20 August 1967, 1300 GMT, orbit 1547. These photographs were made ~12 hr after the OGO-4 data presented in Figs. 5 and 6.

Fig. 5 shows the radiance measurements of three of the photometer channels along the subsatellite track indicated on the ESSA-5 picture. Near 32N where the satellite crossed the North African coast near Sidi Baran, Egypt, the 3914 Å channel did not show any significant response to the drastic change in surface albedo and stayed almost constant across the Sahara Desert to 19N. In the 5577 and 6225 Å channels the coast is marked by a rapid increase of radiance in both channels; the width of the transition zone corresponds to the field of view of the photometer. The peak values over the central desert are above the level measured over the clear ocean by factors of 2.1 for 5577 Å and 3.3 for 6225 Å. Of particular interest are the little peaks observed when passing over the Island of Crete which has a higher albedo than the surrounding water. The absolute values, however, do not reach those over the continent because the island at no time filled the field of view of the photometer.

An interesting fact demonstrating the sensitivity of the photometers is that the measured radiances immediately south of the North African coast and also near 23.5N were considerably lower than over the surrounding desert regions. As can be seen from Fig. 4, the desert north of 30N actually exhibits a lower albedo due to darker sands. Around 23.5N the satellite passes over the Gilf Kebir Plateau which consists of lithosols including brown, chestnut and reddish colors and which even bears some mountain vegetation, both in contrast to the surrounding bare and bright desert sands. In the ESSA-5 photograph this plateau shows some cloudiness in the center which is of orographic origin and will certainly be dissipated during the evening hours. The drop in radiance certainly does not reflect the true albedo change because the plateau did not fill the field of view of the photometer.

From 16 to 19N high values in all three wavelength regions indicate the existence of high-reaching cloud systems which is confirmed by the ESSA-5 daytime photograph. Around 15N the break in the cloud system, as shown in the television picture, is noticeable in the photometer data near the Darfur Mountain where the apparent albedo is equal to that over the northern Sahara Desert (see Fig. 6 which is the southward continuation of Fig. 5). The cloud system detected south of 14N and verified by the daytime photograph seems to increase in height toward the south as can be judged from the steady increase of the radiances measured in all three channels. The sharp southern boundary of the tropical cloudiness observed 12 hr later close to the equator (Fig. 4) can be located near 3N in the OGO-4 data. This difference is quite acceptable if one considers

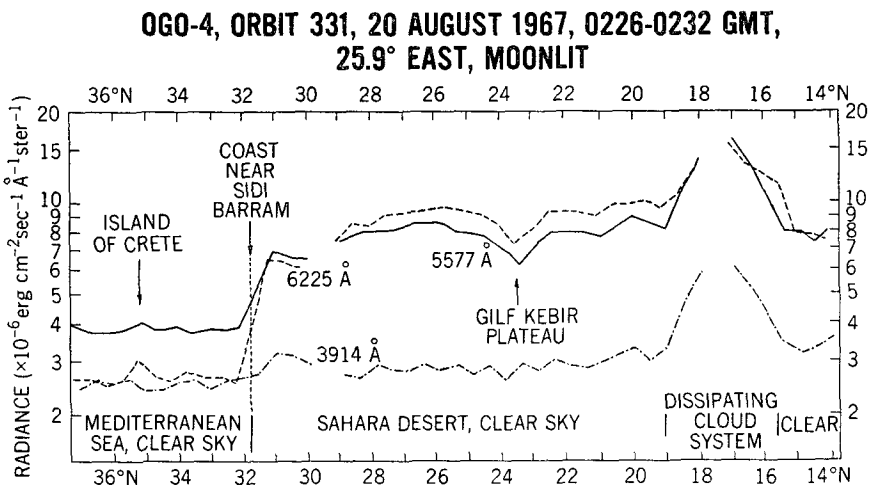

FIG. 5. Observed radiance as a function of geographic latitude over the northern part of the region shown in Fig. 4.

the structure of the tropical cloud systems exhibited in Fig. 4 and taking in account the time difference between both the observations.

In the clear region between 2N and 2S the radiance measurements in the 5577 and 6225 Å channels show about 20–40% lower values than farther north over the clear desert, while the 3914 Å channel shows the same values as before. This indicates the photometer response to the lower albedo over the tropical rain forest of the Congo Basin in comparison with the brighter Sahara Desert.

Over the tropical cloud system the recorded radiances were higher by factors of 4.2, 6.7 and 8.5 in the 3914, 5577 and 6225 Å channels, respectively, compared with the low values over the Mediterranean Sea. Only a small part of this change is due to the change in lunar elevation angle, which was not taken into account in the presented figures.

Farther south, the OGO-4 measurements responded to another tropical cloud system which was confirmed by satellite photographs not included in Fig. 4.

As a second case, an observation over the South Pacific Ocean on 20 August 1967 was selected. The moon was nearly full and at an almost constant elevation of ~33°. The analysis of the photometer measurements are shown in Fig. 8; the corresponding daytime cloud photographs were taken from the ATS-1 satellite 7 hr later (Fig. 7) and from the ESSA-5 satellite (Fig. 9) 12 hr prior to the OGO-4.

A narrow band of high clouds was overflown between 5 and 10S, as indicated by the strong response in all three photometer channels. Clear skies seem to prevail between 11 and 17S in accordance with Fig. 7. South of 18S extended cloud systems were overflown which can be identified as middle altitude cloud decks from the ESSA-5 pictures in Fig. 9. These photographs were taken near sunset, i.e., under a very low solar elevation angle; thus, lower clouds appear darker under the dimmer illumination than higher clouds, and differences can easily be distinguished, particularly between 25 and 30S where higher cloud build-ups are very pronounced in the television photograph. The photometer

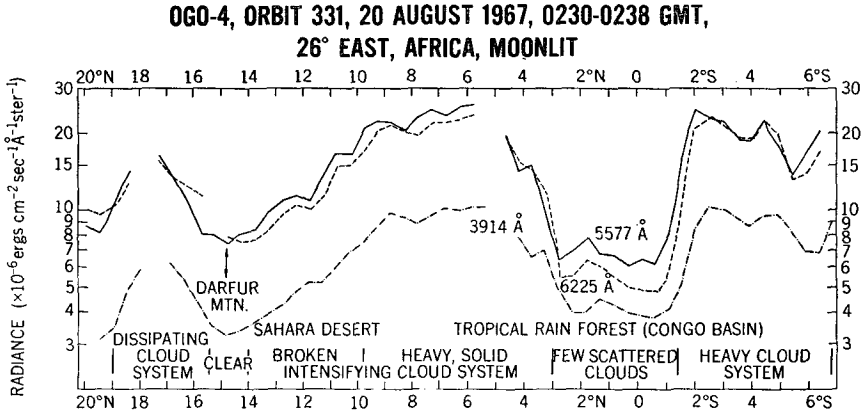

FIG. 6. Observed radiance as a function of geographic latitude over the southern part of the region shown in Fig. 4.

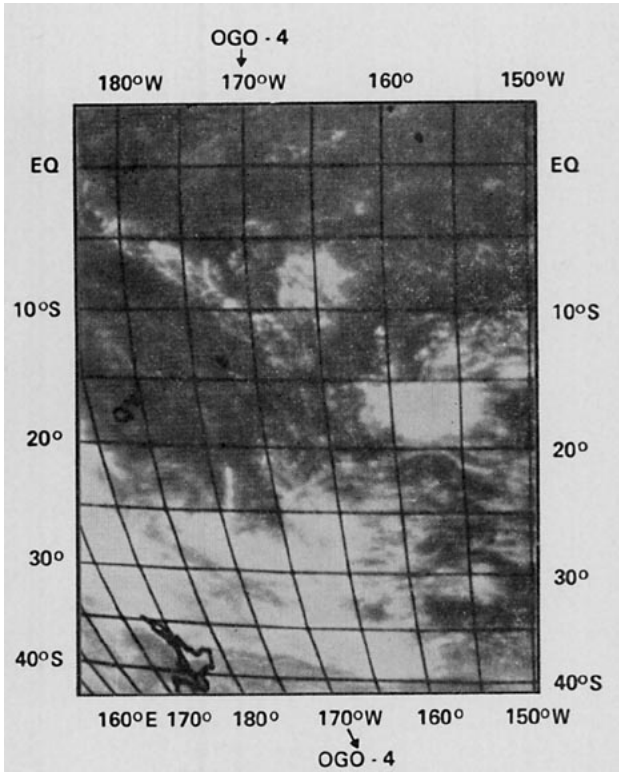

FIG. 7. Path of OGO-4 orbit 339 superimposed on an ATS-1 satellite photograph of a portion of the Pacific Ocean taken ~7 hr after the OGO-4 data presented in Fig. 8.

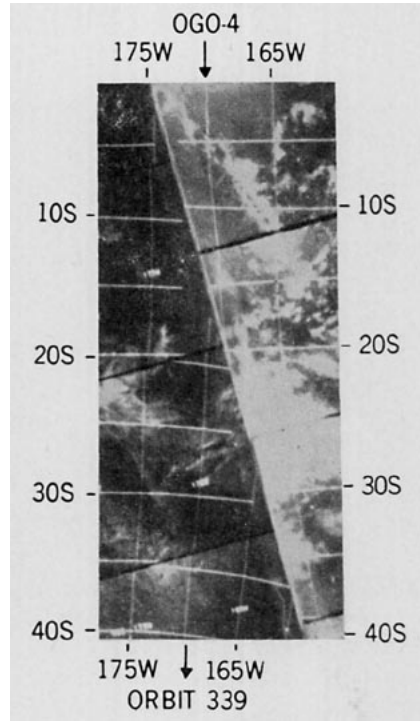

FIG. 9. Path of OGO-4 orbit 339 superimposed on ESSA-5 photographs, 20 August 1967, orbits 1541–0200 GMT and 1542–1400 GMT. These photographs were made ~12 hr prior to data presented in Fig. 8.

measurements also responded to these cloud build-ups as shown by the recorded higher radiances in all three channels. A cloud break at 31–32S, suggested by the drop in all three photometer measurements, can be identified in the satellite photographs as a pre-frontal cloud break along a cold front that had just passed New Zealand. In the post-frontal area of cellular cold air mass convection, south of 37S, the spectral radiances resumed the same values observed over the medium high cloud system 15–20° to the north.

From these moonlight cases it can be concluded that because of the much stronger light source, albedo differences could be detected with even a better degree of separation than without moonlight. The behavior of different spectral intervals with regard to reflector altitude is very obvious and will be discussed in more detail in the next subsection.

3) Analysis of color ratios in terms of cloud characteristics. The data from these examples have been plotted so as to reveal the possibility of obtaining cloud

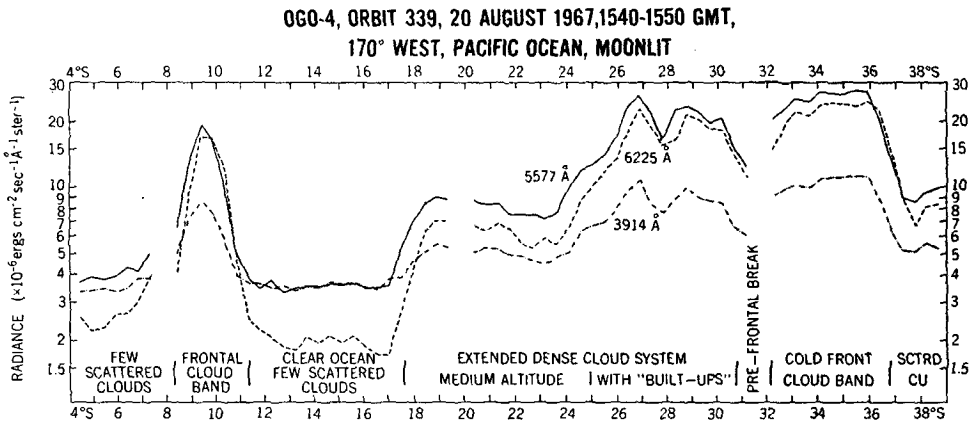

FIG. 8. Observed radiance as a function of geographic latitude over the regions pictured in Figs. 7 and 9.

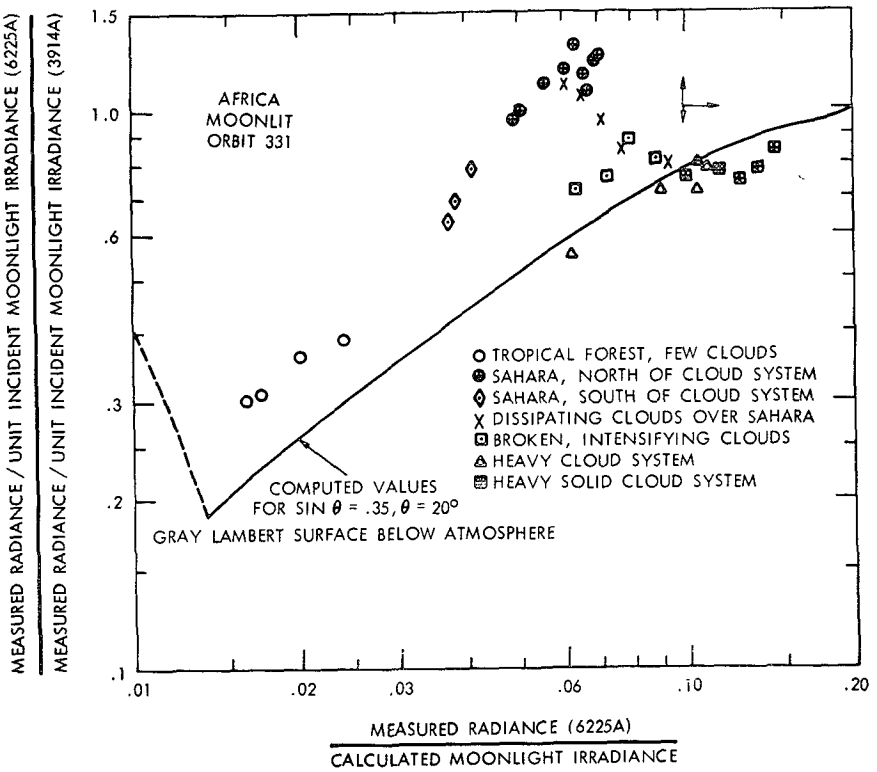

FIG. 10. Analysis of observations of moonlight over Africa. The elevation of the moon ranged from 13° at 32N latitude to 26.5° at 6S latitude.

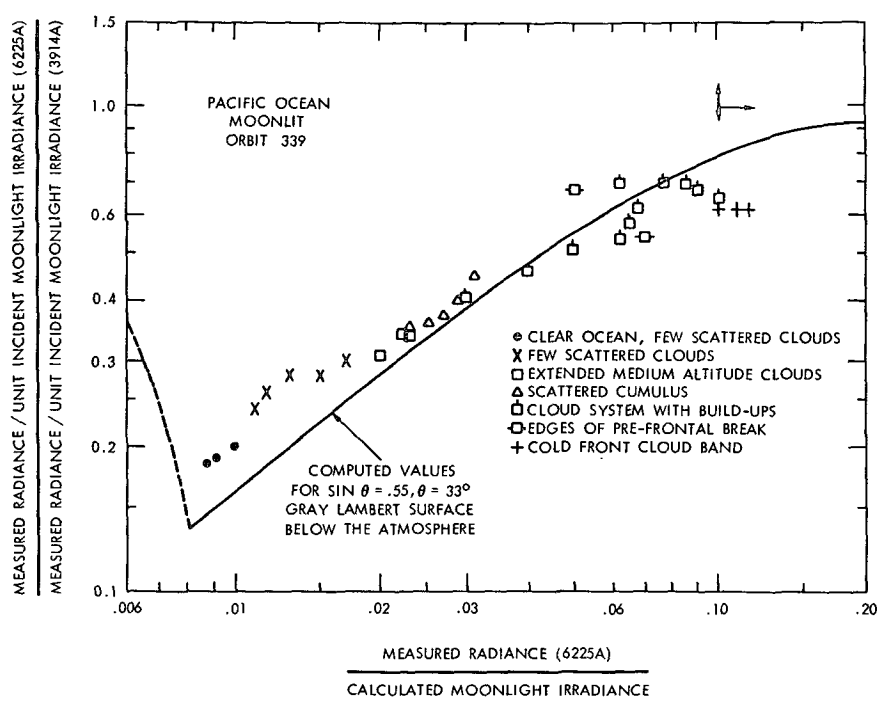

FIG. 11. Analysis of observations of moonlight over the Pacific Ocean. The elevation of the moon was between 32° and 34.5° for these data.

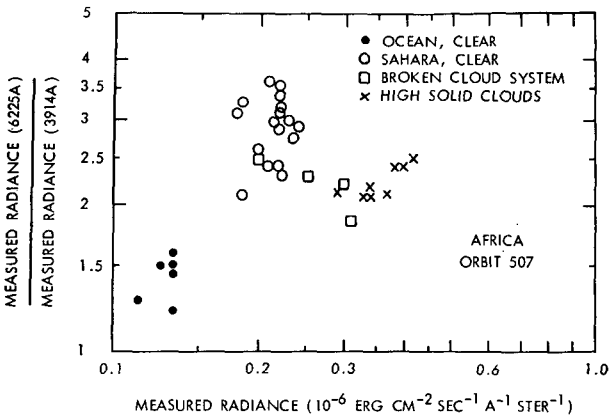

FIG. 12. Analysis of observations of airglow, starlight, zodiacal light, and low level moonlight over Africa. These data have not been adjusted over the spectral content or magnitude of the irradiances.

height information. Data from measurements at 3914 and 6225 Å were used: 3914 Å because Rayleigh scattering is appreciable at this wavelength, 6225 Å because there is relatively little scattering. The data at 6300 Å was not used because the airglow emissions at 6300 Å are markedly enhanced in the equatorial regions; the airglow emission at 6225 Å is more uniform.

In Figs. 10 and 11, the data for the moonlit earth is presented in the same format as were the computations in Fig. 1. The "calculated moonlight irradiance" is the normal component of incident moonlight so that a white lambert surface gives a value of $1/\pi$ for all lunar elevations. When the spacecraft is not in the earth's shadow the contribution due to sunlight scattered from the spacecraft (0.5×10^{-6} erg cm^{-2} sec^{-1} Å^{-1} ster^{-1} for 3914 Å and 2.0×10^{-6} erg cm^{-2} sec^{-1} Å^{-1} ster^{-1} for 6225 Å) has been subtracted from the data in Figs. 3, 5 and 6 to give "measured radiances." The incident moonlight was computed using the solar spectrum given by Thekaekara *et al.* (1969), the lunar albedo given by Harris (1961), and the computed phase, distance and elevation of the moon. The various measurements of the solar spectrum near 3914 Å do not agree, and the vertical arrows in the upper right corner of the figures indicate the uncertainty introduced by the use of other measurements of the solar spectrum (Stair and Johnston, 1956; Dunkelman and Scolnik, 1959).

The absolute calibration of the photometer in orbit has not been carefully studied as yet. The points are plotted on the basis of the laboratory calibration a number of months prior to launch. The use of data from a prelaunch check with calibrated phosphors would move the points as indicated by the horizontal arrow in the upper right corner of the figure. There is some indication from the study of data obtained in orbit that the sensitivity of the photometer did continue to slowly decrease.[3]

[3] A recent evaluation shows in-flight responsivity for the data to have dropped to 70% of the laboratory values.

The various symbols represent the surface and weather conditions as indicated. For comparison purposes, the computed values (Plass and Kattawar, 1968) for a gray lambert surface below the atmosphere are included in Figs. 10 and 11.

From these figures, it is apparent that the observations follow the trend indicated in Fig. 1. The notable, and expected, exception is the Sahara Desert, which is not gray, but has reddish colored sand. There is not as much scatter in the y direction as might be expected due to clouds of varying heights. Possibly few, if any, high clouds happened to fill the field of view of the photometer, or our application of theory is not wholly correct.

In Fig. 12 is plotted the ratio of the observed radiances at 6225 and 3914 Å vs the observed radiance at 6225 Å with various symbols to represent the various surface conditions. Qualitatively, the ocean, the red desert, and the cloudy areas are easily distinguished from each other. These data cannot be directly compared to the computed ratios in Fig. 1 because, first, the observations include the airglow emissions which originate in the atmosphere as well as that reflected from the surface, and second, the source of most of the reflected light is not a point source, but is a nonuniform extended source.

4. Conclusions

From this evaluation of OGO-4 photometric measurements for meteorological purposes it can be concluded: 1) that the illumination of the nightside of the earth is sufficient, even in the absence of moonlight, to detect clouds and certain surface features under clear sky conditions; and 2) that the measurements are sufficiently sensitive to apply the technique of color discrimination in order to derive cloud amount and possibly average cloud top altitude within the field of view.

For a meteorological application, some instrumental changes would be desirable, namely, the photometer should have a narrower field of view and a scanning device. Both requirements seem to be possible by present technology. An additional channel should be provided in a spectral interval containing only auroral emission (e.g., ~2970 Å), in order to detect and eliminate disturbed data.

The results presented in this report have been derived from a relatively small sample of data. However, it is believed that the results are qualitatively correct. Quantitative relationships between the three-dimensional cloud distribution and the multi-spectral photometric measurements have to be established statistically on the basis of a larger volume of data before this method would be quantitatively operational. It is hoped that a further study of the data over snow-covered regions will make it possible to interpret the observed variations in terms of surface ice or snow cover and clouds.

REFERENCES

Dunkelman, L., 1968: The visible and UV scene from space. *J. Opt. Soc. Amer.*, **58**, 731 (abstract).

——, and R. Scolnik, 1959: Solar spectral irradiance and vertical atmospheric attenuation in the visible and ultraviolet. *J. Opt. Soc. Amer.*, **49**, 356–367.

Harris, D. L., 1961: Photometry and colorimetry of planets and satellites. *Planets and Satellites*, Vol. **3**, *The Solar System*, University of Chicago Press, 272–342.

Kondratiev, K. W., Z. F. Mironova, A. N. Otto and V. N. Popova, 1962: The spectral albedo of various surfaces in the visible and near-infrared regions of the spectrum. *Selected Articles from Actinometry, Atmospheric Optics and Nuclear Meteorology, Akad. Nauk Litovskoy SSR; Vilnius.* (Translation: NASA TT F-150, 1964).

Krinov, E. L., 1947: Spektralnaya otrazhatelnaya sposobnost prirodnykh obrazovanii. Moscow. *Laboratoriia Aerometodov, Akad. Nauk SSSR*, 271 p. (Translation: National Research Council of Canada, *NRC-TT-439*, 1953).

Novoseltsev, Y. P., 1964: Spektralnaya otrazhatelnaya oblakov. *Tr. Gl. Geofiziy. Obs.*, No. 152, 186–191. (Translation: Spectral Reflectivity of Clouds, NASA TT F-328, 1965.)

Plass, G. N., and G. W. Kattawar, 1968: Calculations of reflected and transmitted radiance for earth's atmosphere. *Appl. Opt.*, **7**, 1129–1135.

Reed, E. I., and J. E. Blamont, 1967: Some results concerning the principal airglow lines as measured from the OGO-II satellite. *Space Research VII*, Amsterdam, North-Holland Publ. Co., 337–352.

Roach, F. E., 1964: The light of the night sky: Astronomical, interplanetary and geophysical. *Space Sci. Rev.*, **3**, 512–540.

Stair, R., and R. G. Johnston, 1956: Preliminary spectroradiometric measurements of the solar constant. *J. Res. Natl. Bur. Stnds.*, **57**, 205–211.

Suomi, V. E., and R. J. Parent, 1968: A color view of planet earth. *Bull. Amer. Meteor. Soc.*, **49**, 74–75.

Thekaekara, M. P., R. Kruger, and C. H. Duncan, 1969: The solar constant and the solar spectral irradiance measured from a research aircraft. *Appl. Opt.* (in press).